AIAA JOURNAL
Vol. 41, No. 12, December 2003

Drag Reduction by Plasma Filaments over Supersonic Forebodies

V. R. Soloviev,* V. M. Krivtsov,* and A. M. Konchakov*
Moscow Institute of Physics and Technology, Dolgoprudny, Moscow Region, 141700, Russia
and
N. D. Malmuth†
Rockwell Scientific Company, Thousand Oaks, California 91360

Inviscid flow over a supersonic cone-cylinder with thermal plasma filaments projecting upstream of its nose is analyzed numerically. The plasma filaments are idealized as concentric annular layer heat sources. Two limiting cases are assumed. These are, respectively, gas pressure p and gas density ρ constant inside the layers during their formation. For the first case, the drag reduction energetic efficiency remains less than unity for Mach numbers $M = 1.7$–7 for an assumed layer configuration. In the second, the efficiency becomes greater than unity for $M = 2.5$ and reaches its maximum value at $M = 5$ for an optimal layer arrangement. This configuration consists of one central filament and another layer projecting from the cone surface at a radial distance from the cone axis of symmetry one-third of the cylinder radius.

I. Introduction

RECENT experiments[1–3] of supersonic body upstream energy deposition due to different discharges have demonstrated drag reductions that depend on the type of the discharge and its characteristics. Theoretical investigations for the effect of a uniform plasma upstream of a supersonic body qualitatively confirm flow and bow shock modification accompanied by drag reduction.[4,5] However, uniform power input requires too much energy to obtain attractive aerodynamic improvement.

Nonuniform plasma distributions can provide higher energy density, resulting in plasmas with less total input power. Streamer breakdown followed by high-temperature filaments is more practical for atmospheric air than homogeneous glow discharges. The numerical modeling of shock wave (SW) propagation through thermal plasma filaments perpendicular to shocks has shown considerable decrease of the SW intensity.[6] This can be used to weaken forebody bow shocks.

The possibility of filamentary discharges was observed both in still air[7,8] and in supersonic flows[3,9] for radio frequency (RF) electric fields applied to spike electrodes. This interaction usually results in a fluctuating single streamer. Multistreamer discharges are possible using an electrode with an array of small spikes on its surface. For this configuration, the filaments are not randomly distributed over the electrode surface but originate on the spikes of the electrode. Typically, such filamentary structures are avoided in favor of uniform distributions for laser applications. It is important to note that the aforementioned multifilamentary mode has been observed during these investigations.[7]

Self-consistent numerical modeling of multistreamer discharges and their interaction with supersonic airflow is a complex problem. One difficulty is that the streamer evolution to a high-temperature filament has not yet been adequately simulated. Nevertheless, it is possible to make useful aerodynamic benefit assessments of multistreamer discharge configurations with simplified representations of more realistic filamentary arrangements.

It is of interest whether these filaments can remain behind the shock or just touch its rearward side without projecting into the region upstream of itself. If the high-temperature gas filaments "pierce" the shock, the flow modification may be due to disturbance propagation upstream of the shock along the high-temperature subsonic channels, as indicated in Ref. 6. Whether the streamers are upstream or downstream of the shock, the flow can be violently unsteady or a small unsteady modulation on an unsteady flow, depending on how the streamers are produced. Another possibility is that the streamers represent a short impulsive flow. A significant parameter for transient phenomena is a Strouhal number based on the characteristic or evolution time of the streamers compared to the flow convection time. It is conceivable that the Joule heating behind the shock can modify the flow in accord with the Rankine–Hugoniot shock relations. Crocco's theorem indicates that significant changes in vorticity can occur due to entropy gradients normal to the streamlines from the streamers. In this paper, only the shock piercing case is considered.

In many cases, the filaments produced are chaotic, fractal, and tangled "bird's nest" configurations. These have been seen in microwave discharges. On the other hand, collimated, nearly straight filaments are also possible as shown in Ref. 8, where a combination of RF and constant electric field was applied to a spike electrode. This finding as well as the need to estimate any possible aerodynamic benefits motivates the research described in the present paper. Our belief is that nearly straight multistreamer arrangements can be produced to achieve aerodynamic benefits. This paper provides quantitative assessments of such arrangements. Details of their evolution are not emphasized because they require considerable further research, including breakdown and other transient discharge physics. We study such filaments projecting upstream of the nose of an axisymmetric supersonic body. In this framework, the filamentary surfaces are considered as envelopes of straight-line filaments. Accordingly, the surfaces are considered as cylinders concentric with the body axis of symmetry. Bow shock modification and drag changes are emphasized. Quantitative estimates are made of the influence of freestream Mach number, ratio of the interlayer distance to layer width, and the frontal surface area of the cylindrical high-temperature layers.

II. Assessment of Streamer Discharge Filament Parameters

To distinguish different physical phenomena, we use the notations commonly accepted for streamer discharges. A streamer involves propagation of an ionizing wave in a potential gradient. Key features

Presented as Paper 2001-2727 at the AIAA 32nd Plasmadynamics and Laser Conference, Anaheim, CA, 11–14 June 2001; received 12 December 2001; revision received 20 December 2002; accepted for publication 30 August 2003.

*Associate Professor, Department of Applied Physics.
†Senior Scientist and Program Manager, Fluid Mechanics. Fellow AIAA.

exhibited by the streamer are that the gas temperature inside the streamer channel does not vary during streamer propagation and the electron concentration is very high (10^{13}–10^{15} cm^{-3}, depending on gas pressure, the initial potential gradient, and amplitude). The streamer diameter is approximately 0.3–1 mm.

The filament, or stem, denotes the next stage of the streamer discharge development. It is accompanied by gas heating inside the channel and evolution of a self-consistent electrical conductivity inside a channel. The final stage of this development in a unipolar electric field is known as a leader. The gas temperature inside the leader is high enough (4500–5000 K) to maintain air ionization due to the associative ionization reaction $N + O \rightarrow NO^+ + e$ (Refs. 10–12). Existing theoretical analyses deal with single-streamer channel development and streamer-to-leader transition in an impulsive electric field of unchanged polarity.[10–13]

Experimentally, the controlled growth of a high-temperature single filament has been observed by Aints et al. (see Ref. 8, pp. 58–78) for atmospheric air in a RF electric field. These investigations reveal a great contradiction in high-temperature filament development with the predictions of the leader propagation in the unipolar electric field. According to existing theory, the leader in free space of the atmospheric air cannot be created for an electrode potential value less than approximately 300 kV and cannot propagate with a velocity less than $(0.5–1) \times 10^6$ cm/s (Ref. 13). For the spike electrode RF voltage up to 13 kV and electric field frequency $f = 10$ MHz the stem grows with a velocity about 10^3–10^6 cm/s. Here, the observed velocity of stem growth can be considerably less than the minimum velocity predicted for the leader. Furthermore, the amplitude potential value (13 kV) has been observed to be much less than the 300 kV necessary for leader creation in a unipolar electric field at atmospheric pressure.

In the experiments discussed in Ref. 9, high-temperature filament propagation velocity greater than that of a $M = 1.8$ flow has been achieved for $f = 27$ MHz, applied voltage $U_0 \approx 30$ kV, and air pressure $p \approx 100$–150 torr. The temperature in the channel was measured to be nearly 4000 K, and the filament diameter was estimated to be less than 3×10^{-2} cm. These results confirm the contradiction of the stem development in a RF electric field regarding leader formation in an electric field of unchanged polarity. Nevertheless, the main point is that these results confirm the possibility of rapid formation of the high-temperature filaments for relatively low electric field potential values.

On the basis of the experimental results for filament development in RF discharges and existing theoretical models, it seems possible to assume that the gas temperature T_a inside the filaments is of the order of 4000–5000 K, electron density is of the order of 10^{12}–10^{14} cm^{-3}, and electron mean energy $T_e \cong 1$–3eV.

The plasma can be considered as a three-component gas mixture of neutral molecules, electrons, and ions. To describe this system, a multicomponent gas medium approximation is appropriate. It can be characterized by total plasma density ρ, total plasma pressure p, average mass velocity V, and average particle temperature T in the mass, momentum, and energy conservation equations

$$\rho = \sum_{j=a,i,e} m_j N_j \tag{1}$$

$$N = N_a + n_e + n_i, \qquad p = p_a + p_e + p_i \tag{2}$$

$$V = \frac{1}{\rho}(m_a N_a V_a + m_i n_i V_i + m_e n_e V_e) \tag{3}$$

$$T = \frac{1}{N}(N_a T_a + n_i T_i + n_e T_e) \tag{4}$$

where m_a, m_i, and m_e are neutral molecule, ion, and electron mass, respectively; and N_a, n_i, and n_e are their concentrations, respectively.

The effective plasma temperature T for a multicomponent gas mixture representing the plasma is close to the neutral molecule temperature T_a for the aforementioned parameters.

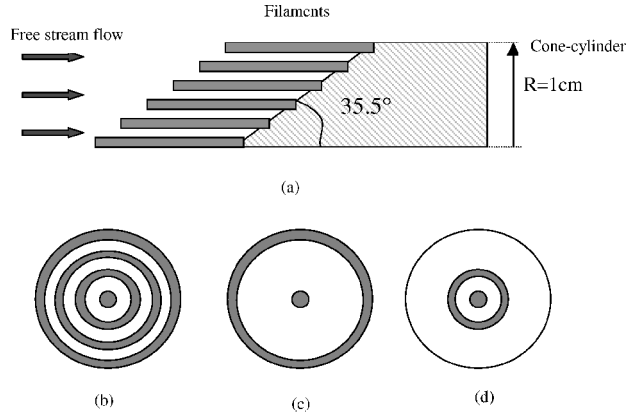

Fig. 1 Physical system of two-dimensional axisymmetrical layer configuration: a) half of longitudinal cross section for equidistant cylindrical layers, b) schematic frontal view of equidistant cylindrical layers in panel a, c) limiting case for $n = 2$ equidistant cylindrical layers, and d) the arbitrary $n = 2$ case for one annular layer with central filament.

III. Statement of Problem

To investigate the possible aerodynamic benefits associated with a filamentary structure in front of a supersonic body, a cone-cylinder body shape was chosen as an example. Concentric cylindrical layers will be assumed to model the filamentary structure. Accordingly, we will hereinafter label these layers as filaments. The distance between the layers, layer width, and filament length will be denoted, respectively, as d, d_s, and l_s. The cylinder radius $R = 1$ cm, and the cone half-angle is 35.5 deg (Fig. 1).

The freestream thermodynamic and the filament parameters remain invariant in all of the calculations and are assumed to be $p_\infty = 0.32 \times 10^5$ Pa, $\rho_\infty = 0.613$ kg/m^3, $T_\infty = 182$ K, and $T_f = 5000$ K.

If the filament channel (cylindrical layer) formation time τ_f is much less than gasdynamic-convection time $\tau_g \sim l_s / V_\infty \sim 10$–$100$ μs, the gasdynamic problem for the effect of the nonuniform filaments forward of a supersonic body can be reduced to an initial-value problem.

A "baseline" inviscid flow pattern that includes a bow shock on the supersonic cone-cylinder is computed for the discharge switched-off condition. We define the discharge switch-on time as $t = 0$. The high-temperature filaments are assumed to be created instantaneously at this time. Accordingly, there is no energy addition (source terms in gasdynamic equations) while the filaments are convected by the incoming freestream flow.

Two contrasting limits are relevant for the establishment of the filamentary environment. The first relates to the $\tau_f < d_s / a_f \sim 1$ μs condition, where a_f = sound velocity inside the filament. In this case the energy deposition into the streamer channel is so fast that the gas density ρ inside the created filament does not change, whereas the gas temperature and pressure increase to $T_f = 5000$ K and $p_f = \rho R_g T_f$, respectively, where R_g is the gas constant. This leads to $t = 0$ initial conditions that in the space between the filaments the conditions remain undisturbed, whereas inside the filaments the gas velocity and density remain undisturbed, but the gas temperature and pressure correspond to filamentary conditions. We call this limit the ρ = const model for filament development.

The other limit corresponds to 1 μs $\sim d_s / a_f \ll \tau_f < \tau_g$. Relatively slow energy deposition into the streamer channel permits the gas to expand from the initial streamer channel boundaries and to equalize the pressure inside the filament with that of the ambient gas. The expanded gas increases the pressure and the density in the filament surrounding area.

For a finite distance between the cylindrical layers, the resultant pressure p after layer formation can be estimated using the mass conservation equation

$$\rho_{\text{in}} S_m = \rho_f S_f + \rho(S_m - S_f) \tag{5}$$

and thermodynamic relations

$$p = \rho R_g T_{\text{in}}, \qquad p_f = \rho_f R_g T_f, \qquad p = p_f \tag{6}$$

where S_f = frontal surface area of the filaments, $S_m = \pi R^2$ is the frontal area of the cone, and the index "in" refers to initial gas parameters before filament formation. Accordingly, $T_{\text{in}} = T_\infty$ ($\rho_{\text{in}} = \rho_\infty$) for the space upstream of the cone bow shock, and T_{in} (ρ_{in}) is the temperature (density) behind the shock for the space region between the bow shock and cone surface. The temperature T_{in} between the filamentary layers is assumed undisturbed in the process of layer formation. From Eqs. (5) and (6)

$$p = p_{\text{in}}\left[1 - \frac{S_f}{S_m}\left(1 - \frac{T_{\text{in}}}{T_f}\right)\right]^{-1} \tag{7}$$

Accordingly, the following initial conditions for the spatial distribution of the gas parameters are relevant for $t = 0$ in this case: For the space between the filaments $T = T_{\text{in}}$ and $\rho = p/(R_g T_{\text{in}})$, whereas inside the filaments $T = T_f$ and $\rho = p/(R_g T_f)$. The flow velocity remains undisturbed, and the pressure p obeys Eq. (7) in all of the space. We designate this limit the $p = \text{const}$ model for filament development.

In the limiting case, corresponding to the interfilament distance being much greater than the filament diameter ($S_f/S_m \ll 1$) and for $T_{\text{in}} \ll T_f$, Eq. (7) gives

$$p - p_{\text{in}} \approx p_{\text{in}} S_f/S_m \to 0$$

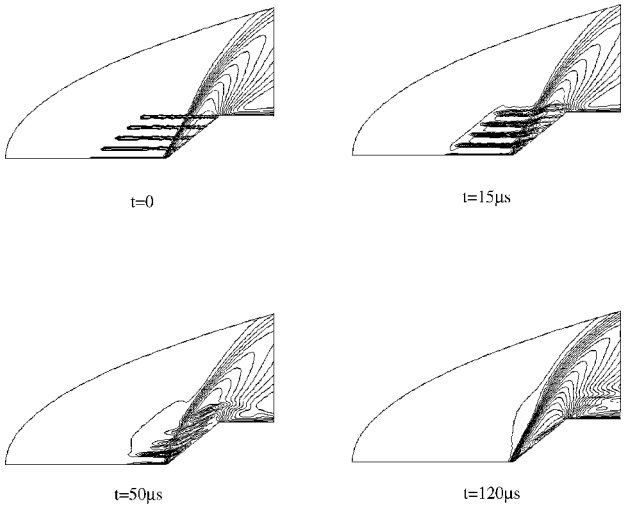

Fig. 2 Mach number contours in the flow around a cone-cylinder for p = const model; $M = 2$, $l_s = 2$ cm, $d_s = 0.5$ mm, and $n = 5$.

This case was considered in our previous paper,[14] and we call this approximation the idealized $p = \text{const}$ model, which does not account for the pressure increase between the filaments at this stage of filament formation.

To obtain a realistic distribution of the gas conditions due to filament production, it is necessary to solve a self-consistent problem of the gas cylindrical expansion forced by the energy extraction inside the filament accounting for kinetics and electrodynamics inside the filament. A complex pattern of cylindrical shocks and rarefaction waves occurs before the pressure inside the filament equalizes to the interfilament pressure. This problem is beyond the scope of this paper and has to be solved elsewhere because the pressure relaxation time can be notably greater than d_s/a_f.

All of the calculations in the aforementioned idealized model to be described were performed using Godunov's second-order accuracy method on a 90×90 grid. The relative computational accuracy was checked with a finer 180×180 grid and was not worse than 5×10^{-3} for mass, momentum, and energy flux conservation inside the computational cell.

The left-top boundary of the computational domain has a parabolic form (Figs. 2 and 3). The flow parameters on this boundary were controlled to coincide with supersonic freestream conditions.

IV. Results and Discussion

Calculated Mach number contours for a freestream Mach number $M = 2$ at different times during the layer convection are shown in Figs. 2 and 3 for the $p = \text{const}$ model and the $\rho = \text{const}$ model, respectively. The layers are situated in a concentric annular arrangement and project forward from the cone surface as shown in Figs. 1a and 1b. In what follows, the number of layers will be denoted as n. The first series of calculations were carried for $n = 5$, $l_s = 2$ cm, $d_s = 0.5$ mm. These are shown in Figs. 2 and 3 where dramatic flowfield modification is evident, especially for the $\rho = \text{const}$ model.

In what follows the drag coefficient will be denoted as

$$c_x = \frac{2}{\rho_\infty V_\infty^2 S_m}\int_S (p - p_\infty)\, ds \tag{8}$$

where ds = cone surface element projection perpendicular to the x axis. Also, the drag change will be considered only for the frontal part of the cone-cylinder body and base drag is ignored.

Our computations show that the effect of drag change persists during the convection time of the filamentary structure. It is evident from them that the time interval for drag reduction increases with filament length l_s. Temporal evolution of the drag coefficient c_x for

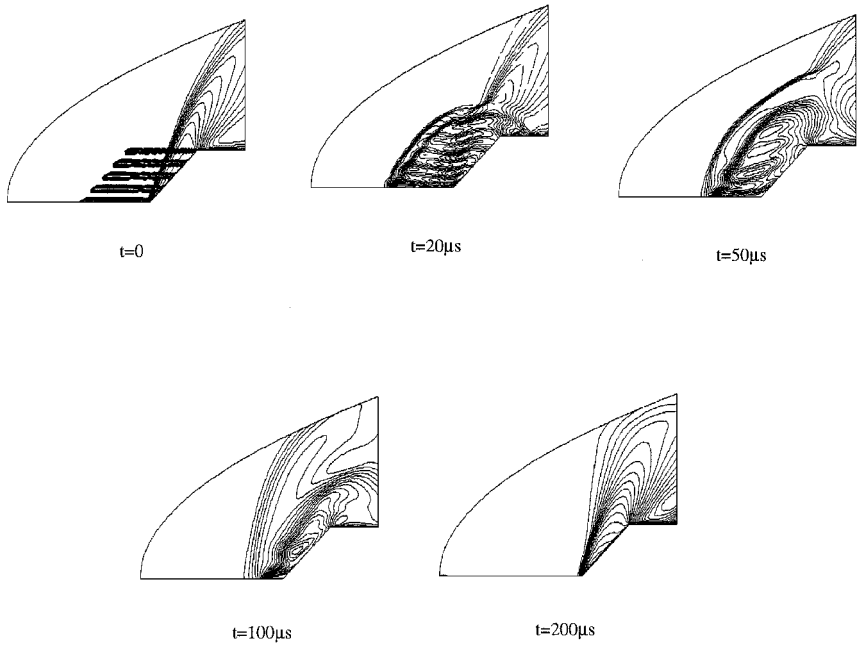

Fig. 3 Mach number contours in flow around a cone-cylinder for ρ = const model; $M = 2$, $l_s = 2$ cm, $d_s = 0.5$ mm, and $n = 5$.

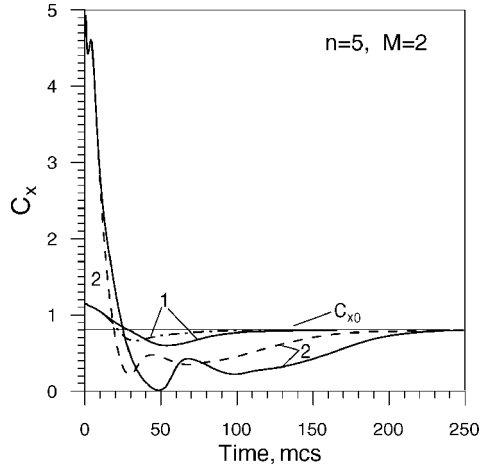

Fig. 4 Drag coefficient vs time for 1, p = const and 2, ρ = const models; d_s = 0.5 mm; – – –, l_s = 1 cm and ——, l_s = 2 cm.

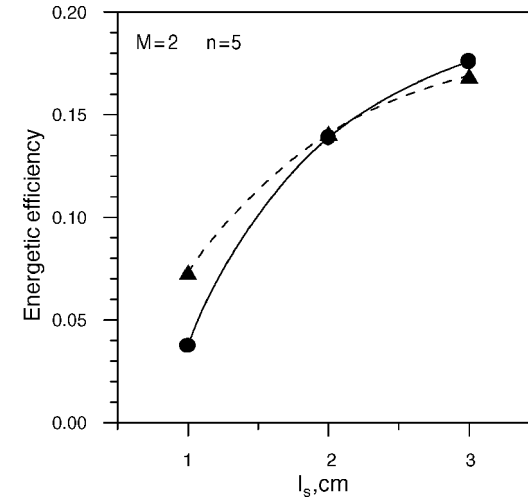

Fig. 5 Drag reduction energetic efficiency vs layer length for p = const (——) and ρ = const (– – –) models; d_s = 0.5 mm.

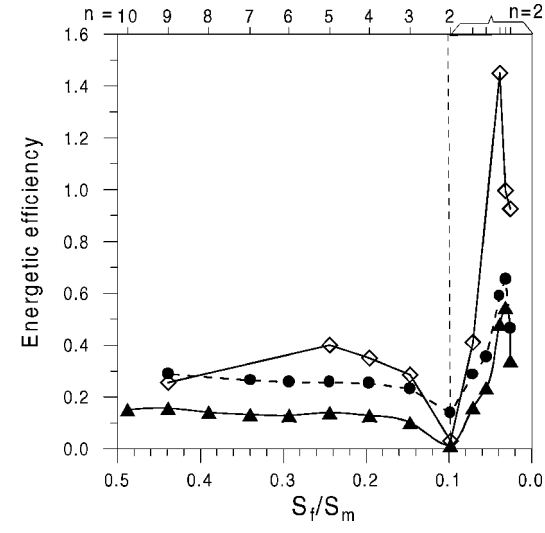

Fig. 6 Drag reduction energetic efficiency vs relative total filament area for d_s = 0.5 mm, l_s = 2 cm: ▲, correct p = const model, M = 2; ●, idealized p = const model[14] (see text), M = 2; and ◇, ρ = const model, M = 6. The layer number n variation from 2 to 10 corresponds to concentric layer configuration covering the entire cone surface starting from the central filament. The n = 2 range describes the central filament with one peripheral annular layer at a different distance from the cone symmetry axis.

the cases presented in Figs. 2 and 3 is shown in Fig. 4 for $l_s = 1$ cm (dashed curves) and $l_s = 2$ cm (solid curves). The initial pressure jump due to high-temperature filament creation induces an initial drag increase, which is much higher for the $\rho = \text{const}$ model than for the $p = \text{const}$ model. However, the subsequent drag decrease is also much greater for the $\rho = \text{const}$ model as shown in Fig. 4.

A power efficiency over time η_E is defined by the ratio of the drag impulsive power to the input power that is necessary to create the relevant filamentary structure Q_f. The drag is integrated over the forebody-projected area in the freestream. Accordingly,

$$\eta_E = \frac{\rho_\infty V_\infty^3 \pi R^2 \int_0^\infty (c_{x0} - c_x)\, dt}{2Q_f} \tag{9}$$

Assume that all of the energy Q_f goes into the gas heating from the initial temperature T_∞ to the final filament temperature T_f. Then, $Q_f = \rho_\infty l_s S_f c_v (T_f - T_\infty)$ for the $\rho = \text{const}$ model. For the $p = \text{const}$ model $dQ_f = \rho l_s S_f c_p dT$, which implies $Q_f = (p/R_g) l_s S_f c_p \ell n(T_f/T_\infty)$. Thus, the final expressions for energetic efficiency are

$$\eta_E = \frac{\gamma(\gamma-1)M^3 T_\infty}{2(T_f - T_\infty)} \times \frac{a_\infty S}{l_s S_f} \int_0^\infty (c_{x0} - c_x)\, dt$$

$$\rho = \text{const} \tag{10}$$

$$\eta_E = \frac{(\gamma-1)M^3}{2\,\ell n(T_f/T_\infty)} \times \frac{a_\infty S}{l_s S_f} \int_0^\infty (c_{x0} - c_x)\, dt$$

$$p = \text{const} \tag{11}$$

where a_∞ is the freestream speed of sound. For the assumed regular structure of the annular concentric layers starting from the central filament projecting from the cone nose (Fig. 1b)

$$S_f = \pi R^2 \frac{d_s}{R}\left[\left(n - \frac{3}{4}\right)\frac{d_s}{R} + n(n-1)\left(1 + \frac{n-1}{n}\frac{d_s}{d}\right)\frac{d}{R}\right] \tag{12}$$

where n = the number of layers on the cone surface (including the central filament), d_s = the width of the layer and the diameter of the central filament, and d = the distance between the layers defined by the equation

$$d = \frac{R - d_s/2}{n-1} - d_s, \qquad n \geq 2 \tag{13}$$

The calculated η_E as a function of the filamentary layer length for $M = 2$, $n = 5$, $d_s = 0.5$ mm is shown in Fig. 5 for $p = \text{const}$ (solid line) and $\rho = \text{const}$ models (dashed line). The cases presented in Figs. 2–4 correspond to the point $l_s = 2$ cm in Fig. 5. The cumulative effect of drag increase and decrease shown in Fig. 4 is almost the same for both models, and the energetic efficiency is substantially less than unity for $M = 2$ and $n = 5$.

Increasing filament length does not change the result dramatically when $l_s > 2R = 2$ cm. Attainment of $l_s > 2R$ appears impractical. To estimate an upper bound to the aerodynamic effect we therefore consider $l_s = 2R = 2$ cm in the computations to be discussed.

To investigate improvement beyond break-even (unity) efficiency, we consider how the layer position and the interlayer distance affect the drag. The most relevant independent variable is the filamentary layer area ratio S_f/S_m.

The dependence of energetic efficiency η_E vs S_f/S_m for the $p = \text{const}$ model is shown by the triangles in Fig. 6 for $M = 2$, $l_s = 2$ cm, $d_s = 0.5$ mm. To vary S_f, we assume the constant $d_s = 0.5$ mm and variable interlayer distance d for equidistant annular layers, with the first filament being at the symmetry axis and the last layer projecting from the edge of the cone surface as shown in Fig. 1b. The number of layers n varies from 10 to 2 corresponding to a S_f/S_m decrease from 0.49 to 0.1. The $n = 2$ case refers to a central filament accompanied by one annular cylindrical layer projecting from the cone-cylinder boundary (Fig. 1c).

The parameter S_f/S_m is decreased further using an annular cylindrical layer approaching the axis of symmetry as shown in Fig. 1d. The domain of validity of results for this case is separated from the aforementioned one by the dashed vertical line in Fig. 6.

The results in Fig. 6 show that if the layers occupy more than 0.15 of the cone surface ($n > 3$ or $d/d_s < 8$), the energetic efficiency weakly depends on S_f/S_m.

For n decreasing from 4 to 2, η_E decreases and reaches its minimum value at $n = 2$ ($S_f/S_m = 0.1$). Further S_f/S_m decrease for central filament and single annular layer approaching the axis of symmetry is accompanied by an efficiency increase until it reaches the maximum value 0.55 at $S_f/S_m = 0.03$ ($d = 2.6$ mm). The most effective energy deposition can be achieved by deploying filaments near the nose of the cone. The radius of this domain is approximately one-fourth to one-third of the body radius for $M = 2$.

The results of the idealized $p = \text{const}$ model[14] for the same parameters are shown in Fig. 6 by circles for comparison with the present more accurate model. Reference 14 can be interpreted as a limiting case within the $p = \text{const}$ model simulation for which the initial pressure jump does not exist. For $M = 2$, both models give $\eta_E < 1$ for all ranges of S_f/S_m and layer configurations.

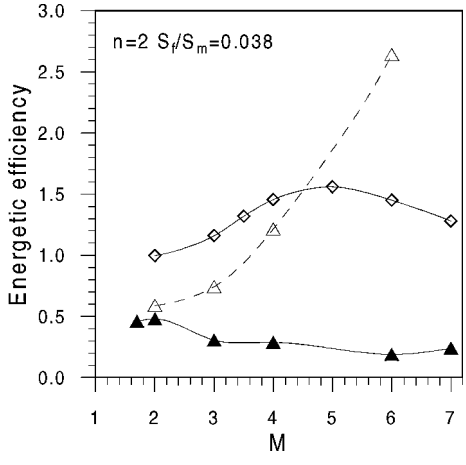

Fig. 7 Drag reduction energetic efficiency dependence on the freestream Mach number for ▲, correct p = const model; △, idealized p = const model[14]; and ◇, ρ = const model; one peripheral annular layer with central filament is upstream of the cone (d_s = 0.5 mm, d = 0.324 cm, l_s = 2 cm, S_f/S_m = 0.0386).

The energetic efficiency dependence on freestream Mach number was analyzed for the $n = 2$, $S_f/S_m = 0.0386$ ($d = 3.28$ mm) layer configuration that consists of a central filament and one annular layer at a distance 0.354 cm from the cone axis. This case gives an η_E greater than that for other layer configurations.

According to Eqs. (10) and (11), the drag reduction energetic efficiency η_E should increase with increasing Mach number, if $\int_0^\infty \Delta c_x dt$ does not decrease dramatically. Figure 7 shows the η_E dependence on freestream Mach number for $p = \text{const}$ (closed triangles) and $\rho = \text{const}$ (diamonds) models. For comparison, the results of the idealized $p = \text{const}$ model[14] (open triangles) are also shown in Fig. 7. A more correct formulation of the $p = \text{const}$ model for the idealized case considered in Ref. 14 results in η_E decreasing with increasing M. Accordingly, the $p = \text{const}$ model gives an energetic efficiency that remains less than unity for all Mach numbers investigated.

For the $\rho = \text{const}$ model, the drag reduction efficiency first increases with the Mach number until reaching its maximum at $M = 5$. For greater Mach numbers, it decreases. The assumed filamentary structure in front of the supersonic body ($n = 2$, $d = 3.28$ mm) is beneficial for $M > 3$ when η_E becomes greater than unity.

The η_E dependence on the filamentary layer arrangement for the $\rho = \text{const}$ model at $M = 6$ is shown in Fig. 6 by diamonds. Greater than unity η_E values can be obtained only for $n = 2$ with a filamentary annular layer projecting from the cone surface in the vicinity of one-third cylinder radius from the cone axis.

The flow field for the $\rho = \text{const}$ model at $M = 4$, corresponding to the $\eta_E > 1$ case, is shown in Fig. 8. For comparison, Fig. 9 shows the flowfield for the $p = \text{const}$ model for the same conditions. The flowfield modification due to forebody filamentary layers is more dramatic for the $\rho = \text{const}$ model. Radial expansion of the high-pressure gas inside layers eats up the bow shock that the body had without the filaments and creates a new complex bow shock structure, as shown in Fig. 8 for the instant $t = 20.5$ μs. This time corresponds approximately to that for the maximum drop of the drag coefficient c_x (Fig. 10; $M = 4$ curve).

The temporal evolution of c_x and η_E is shown in Figs. 10 and 11, respectively, for different freestream Mach numbers. The initial c_x jump is higher for the $\rho = \text{const}$ model (solid curves) than for the $p = \text{const}$ one (dashed curves). However, it is compensated by η_E

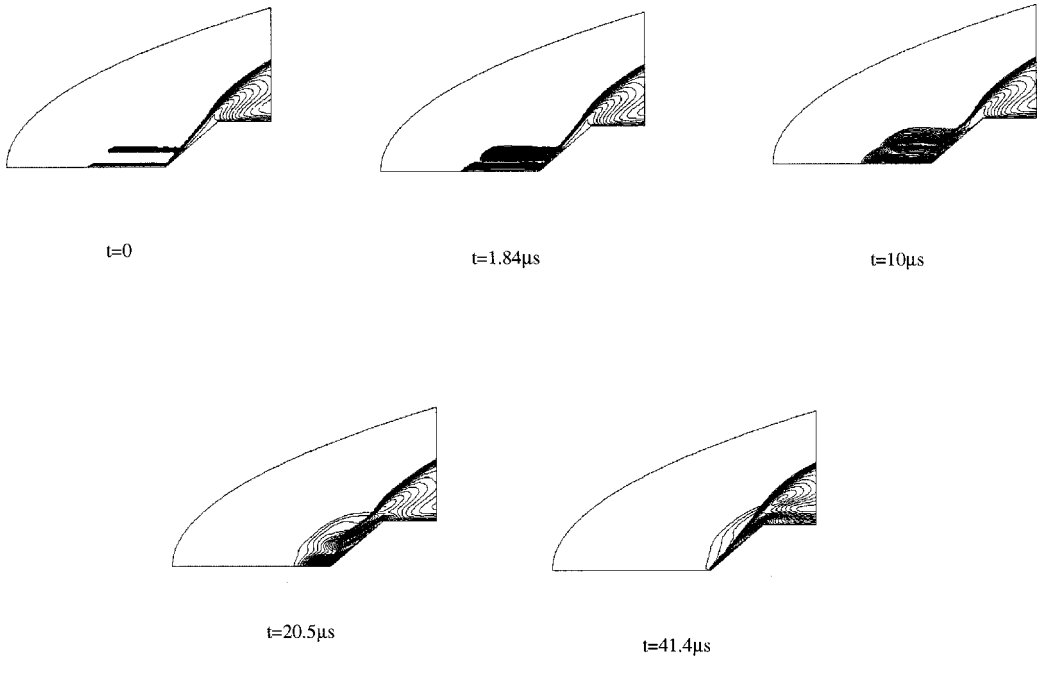

Fig. 8 Mach number contours in the flow around a cone-cylinder for ρ = const model; M = 4, d_s = 0.5 mm, d = 0.324 cm, l_s = 2cm, S_f/S_m = 0.0386, and n = 2 (one annular layer with central filament).

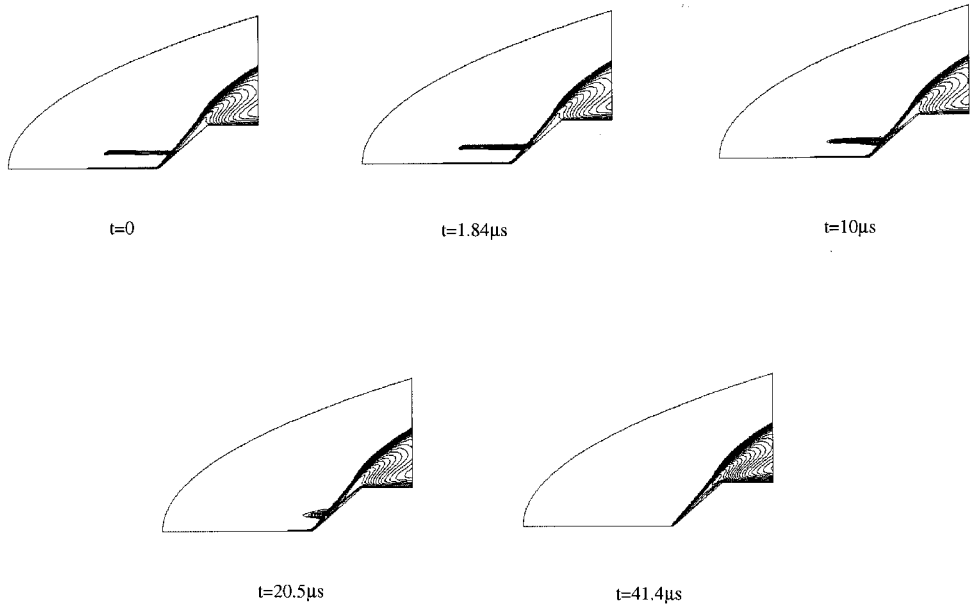

Fig. 9 Mach number contours in the flow around a cone-cylinder for p = const model; $M = 4$, $d_s = 0.5$ mm, $d = 0.324$ cm, $l_s = 2$ cm, $S_f/S_m = 0.0386$, and $n = 2$ (one annular layer with central filament).

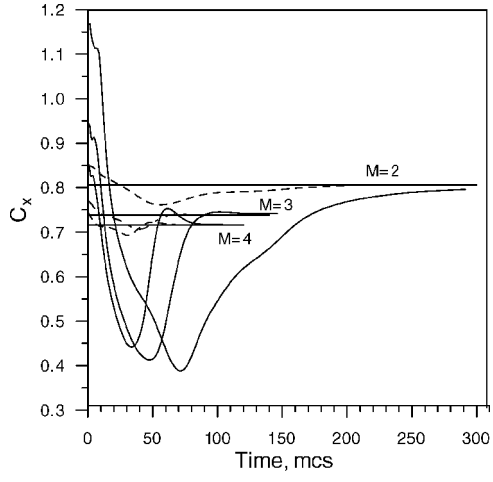

Fig. 10 Drag coefficient temporal behavior for a cone with filaments upstream of itself as in Figs. 8 and 9; ——, ρ = const model and – – –, p = const model ($d_s = 0.5$ mm, $d = 0.324$ cm, $l_s = 2$ cm, and $S_f/S_m = 0.0386$).

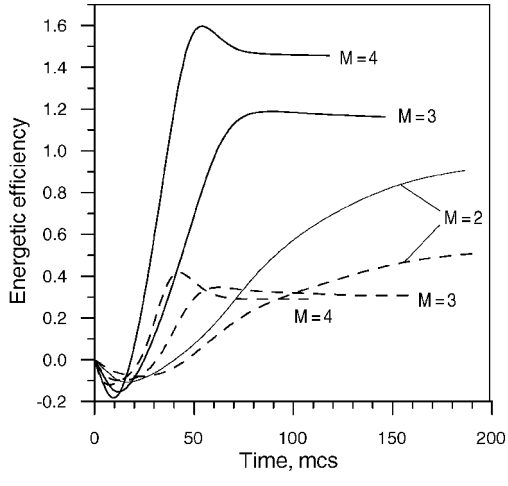

Fig. 11 Energetic efficiency temporal evolution during filamentary convection for freestream Mach number $M = 2$–4; ——, ρ = const model and – – –, p = const model; the layer structure is the same as in Figs. 8 and 9: one peripheral annular layer with central filament ($d_s = 0.5$ mm, $d = 0.324$ cm, $l_s = 2$ cm, and $S_f/S_m = 0.038$).

becoming positive earlier with the $\rho = \text{const}$ model. Additionally, the c_x decrease and filamentary layer convection time are much greater for the $\rho = \text{const}$ model, leading to a higher value of drag reduction efficiency.

The maximum estimated $\eta_E \cong 1.5$ for $M = 5$ is not very impressive. It is notably less than predictions for stationary energy deposition in front of a supersonic body.[4,5] The initial pressure jump and the finite time of the heated domain convection cause this in our unsteady formulation. Continuing energy deposition into the filamentary structure creates a steady flow that could increase the drag reduction efficiency that we conjecture may surpass the η_E values predicted by the idealized $p = \text{const}$ model (Fig. 7), which is free from initial pressure jump.

V. Summary

The inviscid flow around a cone-cylinder supersonic body with forebody filamentary annular layer thermal structure was analyzed numerically. The filament parameters were estimated from existing experimental data and physical models for streamer channel development in streamer discharges.

Two limiting cases were considered for possible high-temperature layer creation corresponding, respectively, to the gas pressure ($p = \text{const}$) and the gas density ($\rho = \text{const}$) remaining constant during this process. The flowfield for both models gives an initial forebody pressure jump that decreases during the layer convection by the incoming flow. The cumulative effect is positive regarding the drag reduction. The maximum drag reduction occurs with a configuration consisting of a central filament and another annular layer projecting from the cone surface at one-third of the cylinder radius distance from the cone axis.

For the $p = \text{const}$ model the drag reduction energetic efficiency remains less than unity for the range of the freestream Mach numbers ($M = 1.7$–7) and the foregoing forebody layer arrangement.

If the energy input into the discharge filament occurs fast enough, the $\rho = \text{const}$ model applies, and the drag reduction energetic efficiency increases with the increasing freestream Mach number until it reaches a maximum of 1.5 for $M = 5$. In this case, the forebody filamentary layer is beneficial for $M > 3$ when the efficiency is greater than unity for the optimal layer arrangement.

Our results show that the hot filament formation processes in streamer discharges are extremely important for aerodynamic application and could result in efficient drag reduction. Efficient and beneficial application could depend on the applied impulse voltage, its time application rate, and the shape of the electrode. This process

should be analyzed carefully to obtain a self-consistent model for streamer discharge aerodynamics improvement.

The results in this paper refer to instantaneous filamentary layer formation followed by the convection of this structure. No energy addition into the filament is considered during the convection process. Low levels of the predicted drag reduction energetic efficiency are due to adverse effect coming from an initial pressure jump. The finite filamentary layer convection time restricts the compensation of this effect by subsequent pressure and drag decrease.

Continuous energy input into a filamentary structure should be analyzed to estimate the drag reduction efficiency for a quasistationary flowfield. In this case, a continuously maintained forebody suction region could result in higher efficiency as compared to that for the transient case studied herein.

From past evidence, it is almost certain that the drag reduction will be less for streamlined bodies than for blunt ones such as the 35.5-deg-half-angle cone considered herein. Because blunt shapes are practically important for hypersonic applications, the appropriate parametric studies were performed in this investigation. Treatment of the streamlined shapes including sharp noses should be performed in the future with the filamentary scheme investigated in this effort.

Numerical simulation of the streamer channel development into hot filament with continuous further energy addition is an extremely complicated problem. Reliable predictions can be obtained only from a triad of experimental, theoretical, and computational effort. Experiments for multistreamer discharge in front of the supersonic bodies are desirable to demonstrate the aerodynamic effectiveness of such a multifilamentary structure.

Acknowledgments

A portion of this effort was sponsored by the Boeing Innovation Research and Development program. Other parts were supported by the Air Force Office of Scientific Research, Air Force Materials Command, under Contracts F49620-92-C-0006 and F49620-96-C-0004. The U.S. government is authorized to reproduce and distribute reprints for government purposes, notwithstanding any copyright notation thereon. The views and conclusions herein are those of the authors and should not be interpreted as necessarily representing the official policies or endorsements, either expressed or implied, of the Air Force Office of Scientific Research or the U.S. government.

References

[1]Bityurin, V., Klimov, A., and Leonov, S., "Assessment of a Concept of Advanced Flow/Flight Control for Hypersonic Flights in Atmosphere," AIAA Paper 99-4820, Nov. 1999.

[2]Leonov, S., Nebolsin, V., and Shilov, V., "Effectiveness of Plasma Effect on Bodies in an Airflow," *Proceedings of the First Russian Workshop on Perspectives of MHD and Plasma Technologies in Aerospace Applications*, IVTAN, Moscow, 1999, pp. 58–65.

[3]Leonov, S., Cain, T., Klimov, A., Pashina, A., Skvortsov, V., and Timofeev, B., "Influence of a HF Corona Plasma Structure on Drag of an Axial-Symmetric Body in a Supersonic Airflow," AIAA Paper 99-4856, Nov. 1999.

[4]Levin, V. A., Afonina, N. E., and Gromov, V. G., "Influence of Energy Input by Electric Discharge Supersonic flows Around bodies," *Proceedings of the 2nd WIG Workshop*, Norfolk, VA, 1998.

[5]Georgievsky, P. Y., and Levin, V.A., "Features of Unsteady Supersonic Flows over Space-Distributed Energy Sources and Sharpen Bodies," AIAA Paper 2001-3053, June 2001.

[6]Soloviev, V. R., Krivtsov, V. M., Konchakov, A. M., and Malmuth, N. D., "Mechanisms of Shock Wave Dispersion and Attenuation in Weakly Ionized Cold Discharge Plasmas," AIAA Paper 99-4908, Nov. 1999.

[7]Korolev, Y. D., and Mesyats, G. A., *Physics of Pulse Breakdown in Gases*, Nauka, Moscow, 1991 (in Russian).

[8]Aronov, M. A., and Larionov, V. P. (eds.) *Electric Isolation of High Frequency High Voltage Devices*, Znak, Moscow, 1994 (in Russian).

[9]Leonov, S., Bityurin, V., and Kolesnichenko, Y., "Dynamics of Single Electrode High-Frequency Plasma Filament in Supersonic Airflow," AIAA Paper 2001-0493, Jan. 2001.

[10]Aleksandrov, N. L., Bazelyan, A. E., Bazelyan, E. M., and Kochetov, I. V., "Modeling of the Long Streamers in Atmospheric Pressure Cases," *Soviet Plasma Physics*, Vol. 21, No. 1, 1995, pp. 60–80.

[11]Aleksandrov, N. L., Bazelyan, E. M., Dyatko, N. A., and Kochetov, I. V., "Streamer Breakdown of the Long Air Gaps," *Soviet Plasma Physics*, Vol. 24, No. 7, 1998, pp. 587–602.

[12]Aleksandrov, N. L., Bazelyan, E. M., Kochetov, I. V., and Dyatko, N. A., "The Ionization Kinetics and Electric Field in the Leader Channel in Long Air Gaps," *Journal of Physics D: Applied Physics*, Vol. 30, 1997, pp. 1616–1624.

[13]Bazelyan, E. M., and Raizer, Y. P., *Spark Discharge*, CRC Press, Boca Raton, FL, 1997, pp. 230–290.

[14]Soloviev, V. R., Krivtsov, V. M., Konchakov, A. M., and Malmuth, N. D., "Simulation of Supersonic Body Drag Reduction Produced by Forebody Filamentary Plasmas," AIAA Paper 2001-2727, June 2001.

G. V. Candler
Associate Editor